

Posterior Annealing: Fast Calibrated Uncertainty for Regression

Uddeshya Upadhyay¹Jae Myung Kim¹Cordelia Schmid^{2,3}Bernhard Schölkopf⁴Zeynep Akata^{1,4}¹University of Tübingen²Inria³Google Research⁴Max Planck Institute for Intelligent Systems, Tübingen

Abstract

Bayesian deep learning approaches that allow uncertainty estimation for regression problems often converge slowly and yield poorly calibrated uncertainty estimates that can not be effectively used for quantification. Recently proposed post hoc calibration techniques are seldom applicable to regression problems and often add overhead to an already slow model training phase. This work presents a fast calibrated uncertainty estimation method for regression tasks, called *posterior annealing*, that consistently improves the convergence of deep regression models and yields calibrated uncertainty without any post hoc calibration phase. Unlike previous methods for calibrated uncertainty in regression that focus only on low-dimensional regression problems, our method works well on a wide spectrum of regression problems. Our empirical analysis shows that our approach is generalizable to various network architectures including, multilayer perceptrons, 1D/2D convolutional networks, and graph neural networks, on five vastly diverse tasks, i.e., chaotic particle trajectory denoising, physical property prediction of molecules using 3D atomistic representation, natural image super-resolution, and medical image translation using MRI images.

1 Introduction

Uncertainty estimation is an essential building block to provide interpretability and secure reliability in modern machine learning systems (Shafaei et al., 2018; Kläs & Vollmer, 2018; Varshney & Alemzadeh, 2017; Hüllermeier & Waegeman, 2021) that offer intelligent solutions for numerous real-world applications, ranging from medical analytics (Leibig et al., 2017; Gillmann et al., 2021; Upadhyay et al., 2021b) to autonomous driving (Xu et al., 2014; Shafaei et al., 2018; Besnier et al., 2021). Recent advances have explored various formulations to provide accurate predictions and uncertainty estimates for deep neural networks, as represented by Bayesian approaches (Gal & Ghahramani, 2016; Kendall & Gal, 2017; Maddox et al., 2019), ensembles (Lakshminarayanan et al., 2016), pseudo-ensembles (Mehrtash et al., 2020; Franchi et al., 2020), and quantile regression (Romano et al., 2019; Yan et al., 2018; Feldman et al., 2021) methods. However, these existing methods are often computationally expensive – e.g., slow convergence rate during training or inefficient inference cost due to multiple forward passes – while being poorly calibrated for uncertainty estimates. Moreover, some of these methods are proposed for low-dimensional regression tasks (Chung et al., 2021; Zhou et al., 2021; Chen et al., 2021) (i.e., regressing a scalar value) and do not scale for high-dimensional regression (i.e., regressing large matrices or tensors). This paper presents a unified formulation to resolve these issues for estimating fast, well-calibrated uncertainty in deep regression models for a wide spectrum of regression problems.

We propose to revisit deep regression models trained via maximum likelihood estimation (MLE), which assumes a Gaussian distribution over the regression output and optimizes the negative log-likelihood to estimate the target and uncertainty. Although such models can ensure low regression error (i.e., high accuracy) and encapsulate the predictive uncertainty, they often converge slowly at the beginning of training due to a flat gradient landscape. Further, they may even risk gradient explosion caused by a steep gradient landscape

when reaching the optima (detailed in Section 3.1), leading to poorly calibrated uncertainty estimates that do not offer credible interpretability for the model.

To reshape the aforementioned ill-posed gradient landscape that causes slow convergence and poorly calibrated uncertainty, we propose a novel *posterior annealing* (POSTA) scheme for deep regression models, that alters the original gradients by formulating a temperature-dependent posterior to be optimized during the learning phase. In contrast to the standard posterior for regression that enforces a fixed Gaussian distribution on the target, we introduce a temperature hyperparameter to impose an evolving distribution.

The proposed temperature-dependent posterior brings crucial properties to regression uncertainty. First, the multimodal distribution on regression target ensures that at high residuals (between output and ground-truth, occurring in the initial learning phase), the gradients are much larger than the standard unimodal Gaussian distribution (explained in detail in Section 3 and Figure 1) leading to faster convergence at the beginning of the learning phase. Second, we also anneal the learning rate over the course of training along with the temperature that avoids gradient explosion towards the end of the learning phase as the posterior distribution evolves to standard unimodal distribution with sharp gradients at lower errors. Third, we construct the temperature-dependent posterior such that the predicted uncertainty is constrained to be calibrated at every step.

The standard unimodal distribution will face slow convergence in the beginning and potential gradient explosion towards the end of the learning phase and provides poorly calibrated uncertainty estimates. In contrast, our POSTA method allows faster convergence and offers well-calibrated uncertainty estimates for a wide spectrum of regressions. This also differs from uncertainty regression methods that estimate the full quantile as they are only shown to be effective on low-dimensional regression.

Contributions. We introduce a temperature-dependent posterior annealing scheme for deep regression models with uncertainty that leads to faster model convergence and offers calibrated uncertainty. We conduct comprehensive evaluation on a wide variety of datasets, including chaotic particle trajectory denoising, physical property prediction of molecules using 3D atomistic representation, image super-resolution, and medical image translation using MRI images.

2 Related Work

Deep neural networks (DNNs) typically estimate inaccurate uncertainty due to their deterministic form that is insufficient for characterizing the accurate confidence (Gal, 2016; Guo et al., 2017). Bayesian inference has been widely studied to effectively estimate uncertainty. Directly performing Bayesian inference on deep nonlinear networks is infeasible due to intractable computations. Hence, approximate inference has been explored by variational inference (Graves, 2011; Blundell et al., 2015; Daxberger et al., 2021; Maddox et al., 2019) or MCMC-based approximation (Welling & Teh, 2011; Chen et al., 2014). However, due to its approximation, the estimated uncertainty may fail to follow the true uncertainty quantification (Lakshminarayanan et al., 2016). Moreover, compared with typical DNNs, approximate Bayesian inference is computationally more expensive and has slower convergence in practice. Non-Bayesian methods have been proposed as an alternative. For instance, (Kendall & Gal, 2017; Lakshminarayanan et al., 2016) modeled two terms, i.e. predictive mean and variance, as an output of DNN to estimate the uncertainty directly from the network’s output. Another line of work estimates the uncertainty in the prediction in a non-parametric manner by estimating different quantiles for a given input (Lin et al., 2021; Chen et al., 2021; Zhou et al., 2021; Chung et al., 2021).

Calibrating the inaccurate uncertainty is another way to estimate accurate uncertainty (Guo et al., 2017). In the regression task, calibration was first defined in a quantile manner (Kuleshov et al., 2018). That is, the estimated credible interval with confidence level α (e.g. 95%) is calibrated if $\alpha\%$ of the ground-truth target is covered in that interval. There are post-processing methods for regression calibration (Kuleshov et al., 2018; Pearce et al., 2018; Tagasovska & Lopez-Paz, 2019). For instance, (Kuleshov et al., 2018) introduced an auxiliary model to adjust the output of the pre-trained model based on Platt-scaling, while others use Gaussian process (Song et al., 2019) or maximum mean discrepancy (Cui et al., 2020). However, an auxiliary model with enough capacity will always be able to recalibrate, even if the predicted uncertainty is completely uncorrelated with the real uncertainty (Laves et al., 2020). Recently, (Levi et al., 2019)

extended the definition of calibration where a regressor is well calibrated if the predicted error is equal to the difference between the ground truth and the predicted mean. Using this definition, (Laves et al., 2020) proposed unbiasing the predicted error by optimizing a scaling factor in the post-processing step. However, such methods often add overhead to an already slow model training phase.

3 Methodology: Posterior Annealing

Our framework that we name Posterior Annealing (POSTA) belongs to the family of models that are designed to predict a distribution for the outputs (Kendall & Gal, 2017; Upadhyay et al., 2021c;a; 2022) and the model is trained via a loss function derived from maximum likelihood estimation (MLE).

In this section, we first describe the problem formulation, discuss related methods and their limitations in Section 3.1. We present posterior annealing method that constructs temperature dependent posterior to learn faster, better-calibrated regression uncertainty in Section 3.2, and analyze the effects of temperature annealing in Section 3.3.

3.1 Background and Motivation

Let $\mathcal{D} = \{(\mathbf{x}_i, \mathbf{y}_i)\}_{i=1}^N$ be the dataset that comprises of samples from domain \mathbf{X} and \mathbf{Y} (i.e., $\mathbf{x}_i \in \mathbf{X}, \mathbf{y}_i \in \mathbf{Y}, \forall i$), where \mathbf{X}, \mathbf{Y} lies in \mathbb{R}^m and \mathbb{R}^n , respectively. The goal of a regression task is to learn a function $\Psi(\cdot; \theta) : \mathbb{R}^m \rightarrow \mathbb{R}^n$ (parameterized by θ) that maps the input \mathbf{x} to the output \mathbf{y} . Let $\hat{\mathbf{y}}_i := \Psi(\mathbf{x}_i; \theta)$ be the estimate for the \mathbf{y}_i and $\epsilon_i := \hat{\mathbf{y}}_i - \mathbf{y}_i$ be the residual between the prediction and the ground-truth. The optimal parameters (θ^*) is learnt by minimizing the error (e.g., ℓ_1 or ℓ_2 loss) between the prediction and ground-truth.

The ℓ_1/ℓ_2 loss function to train regression models originate by treating the residuals (i.e., ϵ_i) as following the i.i.d Laplace/Gaussian distribution. However, the i.i.d assumption will not capture the heteroscedasticity and will not allow uncertainty estimation.

To estimate the uncertainty, the existing works (Kendall & Gal, 2017) relax the i.i.d assumption and learn to model the heteroscedasticity as well. Such models are learned by maximizing the likelihood. Assuming that residuals follow Gaussian distribution, i.e., $\epsilon_i \sim \mathcal{N}(0, \hat{\sigma}_i)$, the likelihood, $P(\mathcal{D}|\theta)$, is a factored Gaussian distribution, $P(\mathcal{D}|\theta) = \prod_{i=1}^N \frac{1}{\sqrt{2\pi\hat{\sigma}_i^2}} \exp(-\frac{|\hat{\mathbf{y}}_i - \mathbf{y}_i|^2}{2\hat{\sigma}_i^2})$. the MLE estimates for the parameters are obtained by minimizing the negative-log likelihood,

$$-\log P(\mathcal{D}|\theta) = \sum_{i=1}^N \frac{\log \hat{\sigma}_i^2}{2} + \frac{|\hat{\mathbf{y}}_i - \mathbf{y}_i|^2}{2\hat{\sigma}_i^2}. \quad (1)$$

The DNN is modified to output both the prediction (i.e., the mean of Gaussian) as well as the uncertainty estimate (i.e., the variance of Gaussian) learned using the above equation, i.e., $\Psi(\mathbf{x}_i; \theta) = \{\hat{\mathbf{y}}_i, \hat{\sigma}_i\}$. While this method allows predicting the uncertainty estimates in single forward pass post training, it has several downsides.

The blue surface in Figure 1 shows the loss from Equation 1 derived by taking negative log of Gaussian likelihood, which consists of two variables: the residual $\mathbf{y}_i - \hat{\mathbf{y}}_i$ (denoted by u) and the standard deviation

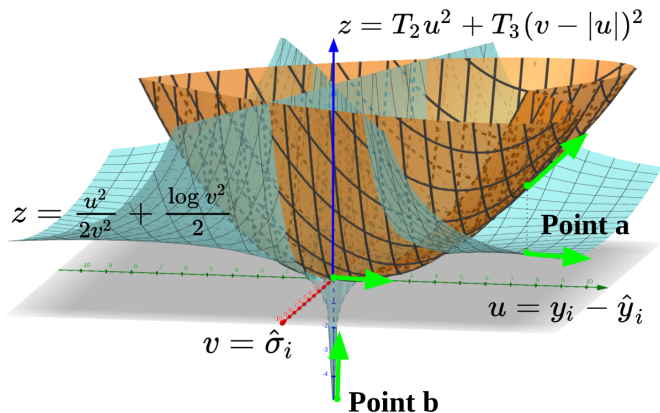


Figure 1: Our temperature dependent loss from Eq2 as a function of residual and the estimated standard deviation (orange surface). In the beginning of the learning phase, the error is high and the gradient of our loss is higher (orange) than the gradient for standard loss (blue). At the end of the training (with close to zero error) the loss function is guided by the standard loss with non-zero gradient, whereas the gradients from the temperature dependent terms become zero.

$\hat{\sigma}_i$ (denoted by v). At the beginning of the training phase, the residual between the prediction and the ground-truth is large but the corresponding gradient at that point is small (see Point a), leading to slower convergence towards optima. As the learning progresses, the residual between prediction and ground-truth reduces substantially with very high gradients leading to gradient explosion (see Point b) if the learning rate is not tuned well. Together, this leads to slower model convergence as gradients in the beginning are too small while the learning rate would also have to be substantially smaller to avoid gradient explosion later. Moreover, (Laves et al., 2020; Levi et al., 2019; Phan et al., 2018) have shown that this method requires an additional post hoc calibration phase as derived uncertainties are miscalibrated.

3.2 Constructing Temperature Dependent Posterior

To tackle the slow convergence issue while providing well-calibrated uncertainty estimates, we formulate a temperature-dependent posterior that facilitates faster convergence with temperature annealing. Our formulation imposes an explicit condition on the uncertainty estimates which are calibrated throughout the learning phase, leading to calibrated uncertainty estimates without any post-hoc calibration phase. We formulate a new posterior distribution on the network output given by,

$$P(\theta|\mathcal{D}) \propto P(\theta) \times \prod_{i=1}^{i=N} \frac{e^{-\frac{|\hat{\mathbf{y}}_i - \mathbf{y}_i|^2}{(2\hat{\sigma}_i^2)}}}{\sqrt{2\pi\hat{\sigma}_i^2}} \times \frac{e^{-T_2(|\hat{\mathbf{y}}_i - \mathbf{y}_i|^2)}}{\sqrt{2\pi\frac{1}{T_2}}} \times \frac{e^{-T_3 \left\{ \begin{array}{l} |\hat{\mathbf{y}}_i - (\mathbf{y}_i + \hat{\sigma}_i)|^2, \hat{\mathbf{y}}_i \geq \mathbf{y}_i \\ |\hat{\mathbf{y}}_i - (\mathbf{y}_i - \hat{\sigma}_i)|^2, \hat{\mathbf{y}}_i < \mathbf{y}_i \end{array} \right\}}}{\sqrt{2\pi\frac{1}{T_3}}} \quad (2)$$

T_2, T_3 are hyper-parameters that we refer to as temperature and $P(\theta)$ is the prior. The maximum a posterior (MAP) of Equation 2 leads to the following loss ($-\log P(\theta|\mathcal{D})$, ignoring constants):

$$-\log P(\theta) + \sum_{i=1}^{i=N} \frac{\log \hat{\sigma}_i^2}{2} + \frac{|\hat{\mathbf{y}}_i - \mathbf{y}_i|^2}{2\hat{\sigma}_i^2} + T_2(|\hat{\mathbf{y}}_i - \mathbf{y}_i|^2) + T_3 \left\{ \begin{array}{l} |\hat{\mathbf{y}}_i - (\mathbf{y}_i + \hat{\sigma}_i)|^2, \hat{\mathbf{y}}_i \geq \mathbf{y}_i \\ |\hat{\mathbf{y}}_i - (\mathbf{y}_i - \hat{\sigma}_i)|^2, \hat{\mathbf{y}}_i < \mathbf{y}_i \end{array} \right\}. \quad (3)$$

With a uniform prior, Equation 3 can be re-written as,

$$-\log P(\theta|\mathcal{D}) = \sum_{i=1}^{i=N} \frac{\log \hat{\sigma}_i^2}{2} + \frac{|\hat{\mathbf{y}}_i - \mathbf{y}_i|^2}{2\hat{\sigma}_i^2} + T_2(|\hat{\mathbf{y}}_i - \mathbf{y}_i|^2) + T_3(|\hat{\sigma}_i - |\hat{\mathbf{y}}_i - \mathbf{y}_i||^2). \quad (4)$$

Figure 2 shows the schematic of our proposed temperature dependent posterior distribution (Equation 2) for a single data point (characterized by $\{\mathbf{y}_i, \hat{\mathbf{y}}_i, \hat{\sigma}_i\}$). The first *temperature dependent* factor in Equation 2:

$$\frac{1}{\sqrt{2\pi\frac{1}{T_2}}} e^{-T_2(|\hat{\mathbf{y}}_i - \mathbf{y}_i|^2)}$$

enforces the central peak in Figure 2, which pushes $\hat{\mathbf{y}}_i$ close to \mathbf{y}_i . The second *temperature dependent* factor in Equation 2:

$$\frac{1}{\sqrt{2\pi\frac{1}{T_3}}} e^{-T_3 \left\{ \begin{array}{l} |\hat{\mathbf{y}}_i - (\mathbf{y}_i + \hat{\sigma}_i)|^2, \hat{\mathbf{y}}_i \geq \mathbf{y}_i \\ |\hat{\mathbf{y}}_i - (\mathbf{y}_i - \hat{\sigma}_i)|^2, \hat{\mathbf{y}}_i < \mathbf{y}_i \end{array} \right\}}$$

ensures that if the prediction $\hat{\mathbf{y}}_i$ deviates from the ground-truth \mathbf{y}_i , then the predicted uncertainty $\hat{\sigma}_i$ is close to the error (i.e., $\hat{\mathbf{y}}_i = \mathbf{y}_i \pm \hat{\sigma}_i$), indicating calibration, which correspond to the left/right peaks.

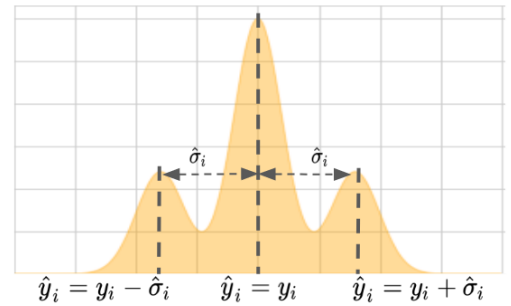


Figure 2: Schematic of the temperature dependent posterior for a single data point characterized by $\{\mathbf{y}_i, \hat{\mathbf{y}}_i, \hat{\sigma}_i\}$. This enforces the prediction to be close to ground-truth and the uncertainty estimate to be close the error, i.e., calibrated.

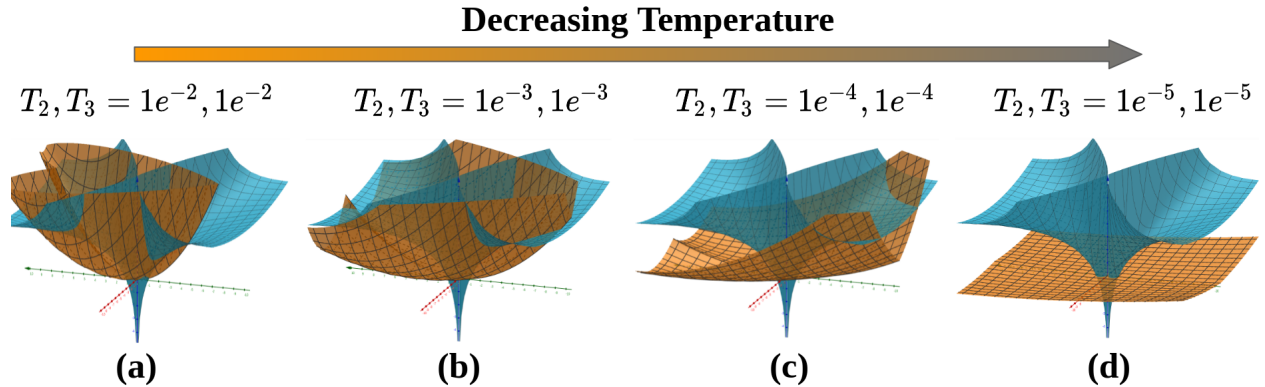


Figure 3: Effects of temperature annealing. As we anneal the temperature in Equation 2, the proposed loss surface (in orange) gradually changes from (a), (b), (c) to (d), which provides faster convergence at the beginning of training while ensuring convergence to the same optima as the standard loss function as described in Equation 1 (in blue).

3.3 Effects of Temperature Annealing

The temperature dependent posterior in Equation 2 allows us to control the contribution of individual loss terms in the final loss Equation 4 by changing the temperature hyper-parameters T_2, T_3 . As described in Section 3, controlling the temperature hyperparameters (i.e., decreasing the values) allows faster convergence of the uncertainty-aware regression with better calibrated uncertainties. We start by initializing T_2, T_3 with a high value of 100 and progressively reduce them according to the training epochs using exponential annealing – referred to as *temperature annealing*.

At higher temperature, the overall loss is dominated by the temperature-dependent loss terms which lead to higher gradients (see Figure 1-(point a on orange curve) and Figure 3(a)). As the temperature decreases, the overall loss is close to the standard loss function given that the gradients from the temperature-dependent terms are close to zero (see Figure 1-(point b on orange surface) and Figure 3 (d)). This dynamic contribution from different loss terms allows the network to converge faster in the beginning (as gradients from the temperature-dependent loss terms are higher than the standard loss term), and ensure stable convergence to the same optima as the standard loss, thus leading to faster, better-calibrated uncertainty.

4 Experiments

We first describe our experimental setup (i.e., datasets, evaluation metrics and implementation details) in Section 4.1. We compare our model to a wide variety of state-of-the-art methods quantitatively and qualitatively in Section 4.2. Finally, we also provide an ablation analysis in Section 4.2 to study the rationale of our model formulation.

4.1 Experimental Setup

Datasets and Tasks. We conduct experiments on five datasets (three small scale problems, two large scale problems) to solve the regression task and provide uncertainty estimation.

We choose the following three low-dimensional regression problems. They highlight the different complexities and network architectures that are required to solve them. In *Chaotic System using Lorenz Attractor (Lorenz Attractor)*, the Lorenz equations describe non-linear chaotic systems given by, $\frac{\partial z_1}{\partial t} = 10(z_2 - z_1)$, $\frac{\partial z_2}{\partial t} = z_1(28 - z_3) - z_2$, $\frac{\partial z_3}{\partial t} = z_1 z_2 - 8z_3/3$. Similar to (Garcia Satorras et al., 2019), to generate a trajectory we run the Lorenz equations with a $\partial t = 10^{-5}$ from which we sample with a time step of $t = 0.05$. Each point is then perturbed with Gaussian noise of standard deviation 0.5 to produce pairs of noisy and clean trajectories split into non-overlapping train/validation/test sets. We use a 1D CNN to map the noisy input

to clean output. The *Physical Properties of Molecules (Atom3D)* (Townshend et al., 2020) is a 3D molecular structure dataset aiming to predict the physical property such as the dipole moment given the 3D atomistic representation. We use the standard Graph Neural Network (GNN) for this task. The *House Price Prediction (Boston-housing)* (Harrison Jr & Rubinfeld, 1978; Belsley et al., 2005) dataset is used to predict the house prices using various attributes using Multi Layer Perceptrons (MLPs).

To show the generalization of our method to high-dimensional regression problems, we use the following two datasets. In *Super-resolution of Natural Images (Super-resolution)*, we learn mapping from low-resolution to high-resolution images using CNNs, using DIV2K dataset (Timofte et al., 2018; Ignatov et al., 2019). We do 4x downsampling to create the corresponding low-resolution images. The dataset is split into 800/100/100 images for training/val/test sets. In *Medical Image Translation (MRI Translation)*, as T1 and T2 MRI from the same patient in the same orientation are often not available and T2 takes longer to acquire, learning a mapping from T1 to T2 is desirable. As in (Upadhyay et al., 2021a), we use T1 and T2 MRI of 500 patients from IXI dataset (Robinson et al., 2010) (200/100/200 for training/val/test) in a 2D CNN based on U-Net (Ronneberger et al., 2015).

Evaluation Metrics. To measure the quality of regression output, we adopt the standard metrics: mean absolute error (MAE) and mean square error (MSE). In addition, for the super-resolution and medical image translation tasks, we use PSNR and SSIM to measure the structural similarity between two images (Wang et al., 2004). To measure the quality of uncertainty estimates ($\hat{\sigma}^2$), we compute (i) the correlation coefficient (Corr. Coeff.) between uncertainty estimates ($\hat{\sigma}^2$) and the error ($|\hat{\mathbf{y}} - \mathbf{y}|^2$). (ii) *Uncertainty calibration error* (UCE) for regression tasks (Laves et al., 2020; Levi et al., 2019). Following (Guo et al., 2017), the uncertainty output $\hat{\sigma}^2$ of a deep model is partitioned into M bins with equal width (each represented by B_m for $\forall m \in \{1, 2 \dots M\}$). A weighted average of the difference between the predictive error and uncertainty is used, $\text{UCE} = \sum_{m=1}^M \frac{|B_m|}{N} |\text{err}(B_m) - \text{uncer}(B_m)|$. Where, $\text{err}(B_m) := \frac{1}{|B_m|} \sum_{i \in B_m} \|\hat{\mathbf{y}}_i - \mathbf{y}_i\|^2$ and $\text{uncer}(B_m) := \frac{1}{|B_m|} \sum_{i \in B_m} \hat{\sigma}_i^2$. (iii) UCE for the re-calibrated uncertainty estimates (R.UCE). We use post-hoc calibration technique introduced in (Laves et al., 2020), called σ -scaling, that optimizes for the scaling factor (s), post training to produce uncertainty estimates ($\hat{\sigma}^2$) and predictions ($\hat{\mathbf{y}}$) using, $s^* = \underset{s}{\text{argmin}} \left[N \log(s) + \frac{1}{2s^2} \sum_{i=1}^N \frac{|\hat{\mathbf{y}}_i - \mathbf{y}_i|^2}{\hat{\sigma}_i^2} \right]$. In addition, we present the (iv) *expected calibration error* (ECE) and (v) *sharpness* (Sharpness). While ECE is another metric to quantify the calibration of the uncertainty estimates, one must note that it may be possible to have an uninformative, yet average calibrated model (Chung et al., 2021; Zhou et al., 2021). Therefore it is necessary to also present the Sharpness metric that encourages more-concentrated distributions. Finally, we present the (vi) predictive log-likelihood that assesses how well the predicted conditional distribution fits the data.

Implementation Details. Our POSTA method is generalizable across different types of architectures. Here we perform experiments with MLPs, 1D/2D CNNs, and GNNs. We take the well-established networks for the respective problems and modify them to produce the uncertainty estimates as described in (Kendall & Gal, 2017; Sudarshan et al., 2021). All the networks were trained using Adam optimizer (Kingma & Ba, 2014). The initial learning rate was set to $2e^{-4}$ and cosine annealing was used to decay the learning rate over the course of the learning phase. The hyper-parameters, (T_2, T_3) (Equation 4) were set to (100, 100) and scheduled to exponentially decay over the course of the training. We provide the code in the supplementary.

4.2 Comparing to Uncertainty Estimation Methods

Compared methods. For each of the regression tasks, we compare our model (POSTA) to eight representative state-of-the-art methods for uncertainty estimation using DNNs for regression tasks, belonging to a diverse class of methods, i.e. Bayesian, ensemble, test-time data augmentation, maximum likelihood, and finally quantile regression methods.

Bayesian methods: In (DO) (Gal & Ghahramani, 2016) the weights of the neural network are randomly dropped at training and inference time. Multiple forward passes for the same input at inference time allow us to estimate the uncertainty. In Concrete Dropout (Conc. DO.) (Gal et al., 2017) the optimal dropout probability for the weights of the neural network are learnt at training.

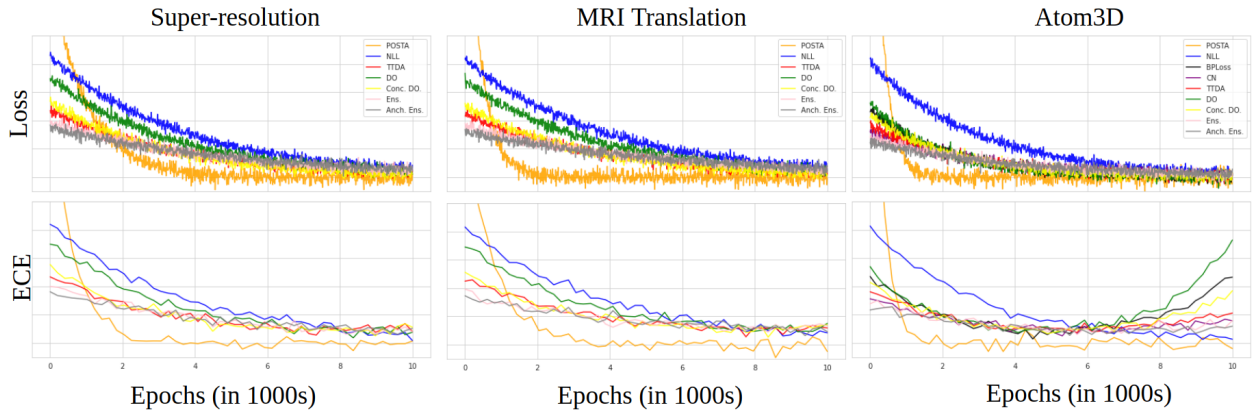


Figure 4: Plots comparing the required convergence time (number of epochs to converge) for different methods and corresponding ECE during the training on (i) Super-resolution, (ii) MRI translation, (iii) Atom3D. More results in supplementary.

Ensemble Methods: In Deep Ensemble (Ens) (Lakshminarayanan et al., 2016) multiple deterministic networks are trained to make the final prediction with uncertainty estimates. In Anchored Ensemble (Anch. Ens.) (Pearce et al., 2020) the weights of the neural networks in the ensemble are regularized about values drawn from a prior distribution, allowing approximate Bayesian inference.

Test-time Data Augmentation Methods: In Test Time Data Augmentation (TTDA) (Wang et al., 2019; Ayhan & Berens, 2018; Gawlikowski et al., 2021) multiple perturbed copies of the input are passed through a deterministic network to estimate the predictive uncertainty at the inference stage.

Maximum likelihood methods: In this method (NLL) (Kendall & Gal, 2017; Sudarshan et al., 2021) the network is modified to predict the mean and variance and then trained by optimizing negative log-likelihood. The variance head then provides uncertainty estimates for the prediction at the inference time.

Quantile Regression Methods: In Calibrated Quantile Regression Method (BPLoss) (Chung et al., 2021) proposes a model that specifies the full quantile function for the predictions and achieves a balance between calibration and sharpness. In Collaborating Networks for estimating uncertainty intervals (CN) (Zhou et al., 2021) two networks are trained simultaneously, one to estimate the cumulative distribution function, and the other approximates its inverse. We note that some baseline methods (i.e., BPLoss and CN) have only been proposed for low-dimensional regression settings (where the output of a model is single scalar) and it is non-trivial and inefficient to scale it to high-dimensional regression settings (e.g., image translation, where the output for an input is a high-dimensional matrix/tensor). Therefore such models are compared only on low-dimensional regression tasks where they are applicable.

Quantitative results on convergence. In this experiment, we train different models to perform the different kinds of regression task and keep track of the training and validation loss to identify if the model has converged. For all the models we used the same optimizer (i.e., Adam (Kingma & Ba, 2014)) with the same initial learning rate (i.e., $1\mathbf{r}=2e^{-4}$) and identical decaying schedule (i.e., cosine annealing for $1\mathbf{r}$).

We observe in Figure 4 that the baseline methods consistently take longer time to converge while our proposed method (POSTA) consistently has faster convergence. For instance, on the super-resolution task, our method takes about 4,000 epochs to converge while the other baseline methods consistently take longer than 8000 epochs to converge. In particular, the NLL baseline takes the longest to converge. We also note that in the early phase of training, our POSTA has much higher loss, this is due to the additional temperature dependent loss terms (in Equation 4) that contribute to the overall loss. However, the higher values of the temperature T_2 and T_3 in the beginning of the training phase also allow faster convergence, as explained in Section 3. Moreover, towards the end of the training phase, the temperature parameters are annealed to a low value (close to zero) and the over all loss function reduces to a low value.

T	Methods	Metrics										
		MAE ↓	MSE ↓	SSIM ↑	PSNR ↑	C.Coeff. ↑	UCE↓	R.UCE↓	Log-likeli. ↑	ECE ↓	Sharp. ↓	
Boston-housing	DO (Gal & Ghahramani, 2016)	2.851	13.26	-	-	0.014	10.76	10.18	-2.46	10.2	8.66	
	Conc. DO (Gal et al., 2017)	2.413	10.18	-	-	0.135	9.882	9.126	-2.15	9.18	9.16	
	Ens. (Lakshminarayanan et al., 2016)	2.971	13.76	-	-	0.011	11.26	10.78	-2.41	10.3	8.87	
	Anch. Ens. (Pearce et al., 2020)	2.553	10.11	-	-	0.154	9.547	9.135	-2.32	9.92	9.82	
	TTDA (Wang et al., 2019; Ayhan & Berens, 2018; Gawlikowski et al., 2021)	2.584	10.30	-	-	0.007	14.32	13.85	-2.24	11.8	9.28	
	NLL (Kendall & Gal, 2017)	2.663	10.75	-	-	0.107	12.67	12.23	-2.42	11.5	8.21	
	BPLoss (Chung et al., 2021)	2.684	11.49	-	-	0.237	9.216	8.837	-2.11	9.72	9.01	
	CN (Zhou et al., 2021)	2.594	11.13	-	-	0.213	10.84	9.722	-2.23	9.65	9.67	
	POSTA (ours)	2.593	10.51	-	-	0.348	0.756	6.374	-2.06	6.37	8.22	
	Atom3D	DO (Gal & Ghahramani, 2016)	1.950	5.828	-	-	0.085	5.380	5.054	-0.24	2.12	4.32
Conc. DO (Gal et al., 2017)		1.834	5.212	-	-	0.136	4.879	4.122	-0.21	1.81	4.18	
Ens. (Lakshminarayanan et al., 2016)		1.215	2.388	-	-	0.138	4.623	4.376	-0.23	1.69	4.17	
Anch. Ens. (Pearce et al., 2020)		1.087	1.743	-	-	0.182	4.124	3.763	-0.26	1.42	3.95	
TTDA (Wang et al., 2019; Ayhan & Berens, 2018; Gawlikowski et al., 2021)		0.903	1.301	-	-	0.157	4.167	3.988	-0.38	1.94	4.78	
NLL (Kendall & Gal, 2017)		0.498	0.463	-	-	0.164	3.358	3.335	-0.22	1.38	3.32	
BPLoss (Chung et al., 2021)		0.527	0.873	-	-	0.189	3.527	3.166	-0.21	1.55	3.12	
CN (Zhou et al., 2021)		0.521	0.845	-	-	0.087	4.311	2.971	-0.16	1.77	3.18	
POSTA (ours)		0.513	0.495	-	-	0.567	0.296	0.277	-0.18	1.37	3.17	
Lorenz Attractor		DO (Gal & Ghahramani, 2016)	1.373	3.463	-	29.85	0.281	2.864	2.134	-0.16	4.34	5.67
	Conc. DO (Gal et al., 2017)	1.247	3.198	-	30.34	0.311	2.379	2.136	-0.14	4.13	5.22	
	Ens. (Lakshminarayanan et al., 2016)	2.544	11.65	-	24.32	0.778	6.726	6.294	-0.22	10.4	8.43	
	Anch. Ens. (Pearce et al., 2020)	2.122	10.12	-	25.64	0.432	8.756	8.154	-0.29	10.7	9.43	
	TTDA (Wang et al., 2019; Ayhan & Berens, 2018; Gawlikowski et al., 2021)	1.391	3.764	-	29.16	0.438	3.325	3.077	-0.17	5.96	8.91	
	NLL (Kendall & Gal, 2017)	0.172	0.048	-	31.28	0.588	2.368	1.933	-0.13	4.33	7.87	
	POSTA (ours)	0.153	0.029	-	32.33	0.821	0.779	0.356	-0.11	4.36	9.12	
	Super-resolution	DO (Gal & Ghahramani, 2016)	0.832	0.548	0.947	35.64	0.033	0.748	0.519	-0.38	4.67	6.32
		Conc. DO (Gal et al., 2017)	0.801	0.423	0.951	35.71	0.134	0.711	0.494	-0.36	4.43	8.82
		Ens. (Lakshminarayanan et al., 2016)	0.793	0.462	0.953	36.61	0.029	0.941	0.733	-0.36	8.76	10.2
Anch. Ens. (Pearce et al., 2020)		0.755	0.441	0.957	36.63	0.178	0.883	0.713	-0.41	8.11	9.21	
TTDA (Wang et al., 2019; Ayhan & Berens, 2018; Gawlikowski et al., 2021)		0.883	0.691	0.939	34.94	0.047	1.175	0.994	-0.39	11.3	10.3	
NLL (Kendall & Gal, 2017)		0.693	0.414	0.955	37.15	0.189	0.581	0.512	-0.36	1.45	2.73	
POSTA (ours)		0.618	0.351	0.962	37.87	0.518	0.104	0.053	-0.16	0.74	0.83	
MRI Translation		DO (Gal & Ghahramani, 2016)	0.732	0.683	0.912	32.45	0.159	0.864	0.771	-0.33	4.48	6.23
		Conc. DO (Gal et al., 2017)	0.715	0.612	0.917	32.97	0.189	1.125	0.932	-0.31	4.12	7.89
		Ens. (Lakshminarayanan et al., 2016)	0.681	0.611	0.927	33.76	0.110	1.143	0.974	-0.36	4.86	7.21
	Anch. Ens. (Pearce et al., 2020)	0.655	0.532	0.933	33.84	0.166	1.122	0.913	-0.34	5.88	7.32	
	TTDA (Wang et al., 2019; Ayhan & Berens, 2018; Gawlikowski et al., 2021)	0.755	0.729	0.904	32.18	0.128	1.483	1.153	-0.37	7.21	9.74	
	NLL (Kendall & Gal, 2017)	0.632	0.582	0.938	34.34	0.134	1.673	1.448	-0.28	4.03	5.12	
	POSTA (ours)	0.615	0.537	0.946	35.27	0.432	0.098	0.062	-0.30	3.26	5.78	

Table 1: Evaluating different methods on five datasets using MAE, MSE, PSNR, SSIM (where applicable, to evaluate regression) and C.Coeff., UCE, R.UCE, Log-Likeli., ECE, Sharp. (to measure quality of uncertainty estimates). ↑/↓ indicates higher/lower is better. “T”: tasks. Best results are in **bold**.

Figure 4 (second row) shows the evolution of ECE for the derived uncertainty using various methods during the training. Again we see that our POSTA achieves the lowest ECE much faster than the other methods. A similar trend is observed for the other datasets. For example, on Atom3D dataset, the proposed method converges at about 2000 epochs, much faster than other baselines, similarly it achieves lowest ECE much faster than other methods. These results show that our method converges much faster than the other methods, which is in line with our motivation to ensure a faster convergence for regression uncertainty model along with better calibrated uncertainty as described in Section 3.3.

Quantitative results on regression and uncertainty. Uncertainty-aware regression models must be evaluated on two fronts which are (i) the regression performance, i.e., the quality of the target predictions and (ii) the quality of estimated uncertainty (the uncertainty should be sharp and well calibrated). We evaluate the model performance based on two set of metrics: (1) task-specific metrics that evaluate the regression results using MAE, MSE, PSNR, SSIM, and (2) calibration-specific metrics that evaluate the quality of the uncertainty estimates using C.Coeff., UCE, R.UCE, ECE, Sharp., and Log-likeli. Table 1 shows the quantitative results that evaluate regression and the quality of uncertainty estimates for different methods on multiple regression tasks. Our POSTA method also obtains high quality regression outputs. In two tasks (including super-resolution, and MRI translation), our POSTA achieves the best or competitive performance compared to the other methods. We note that while no single metric can indicate the “goodness” of uncertainty estimates (as there is no groundtruth for uncertainty values), the collective set of metrics such as C.Coeff., UCE, R.UCE, ECE, Log-likeli, Sharp. provide a holistic indication of “goodness” of uncertainty metric. The proposed method, POSTA, consistently performs well in terms of the above metrics. Overall, these quantitative results show that our method performs well in providing both satisfactory regression results and uncertainty estimates.

Qualitative results on regression and uncertainty. Figure 5 shows the regression output on different datasets. Figure 5-(i) & (ii) visualizes the generated images for image super-resolution and MRI translation

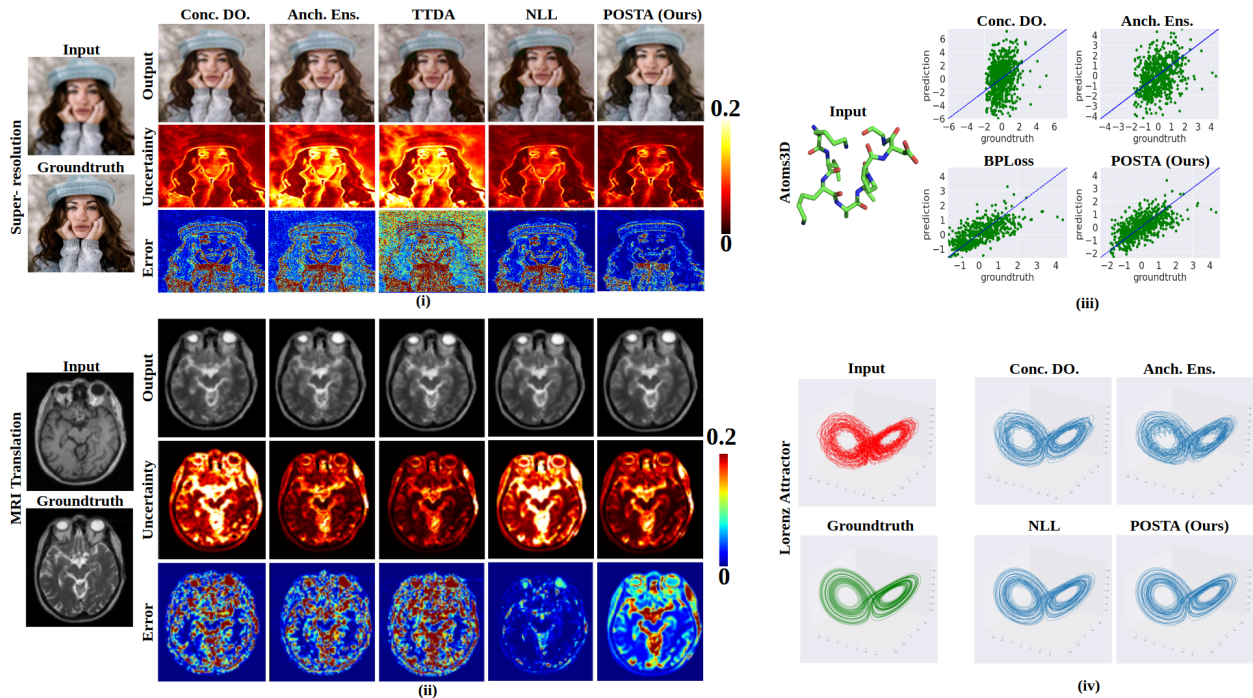


Figure 5: Qualitative results: input, predictions, groundtruth, and the error.

tasks. While the other methods often generate relatively blurry images with artifacts in colours, our model produces better output visually more similar to the ground-truth. Moreover, Figure 5-(i) & (ii) also shows the uncertainty maps, along with the prediction and error for super-resolution and MRI translation. We observe that for compared methods, uncertainty maps do not always agree with error maps at pixel level (i.e., higher/lower uncertainty than the corresponding error), whereas our uncertainty maps are in agreement with the errors. This suggests that our model provides better-calibrated uncertainty. Figure 5-(iii) shows the plots for predictions vs ground-truth on the Atom3D dataset. We can see that compared to other methods, our method yields predictions much closer to the ground-truth e.g., on the Atom3D dataset, our method produces regression output more highly correlated with the ground-truth. Figure 5-(iv) shows the input noisy trajectory, denoised output and the corresponding ground-truth for the Lorenz attractor dataset. We can see that compared to other methods, our method yields smoother trajectories.

4.3 Ablation Analysis of Posterior Annealing

Table 2 shows the ablation study of two temperature hyperparameters in our formulated temperature dependent posterior (Equation 2) along with different choices of priors for the super-resolution task.

We test the baseline that removes both temperature dependent terms (i.e. $T_2 = T_3 = 0$) with a uniform prior, this is equivalent to the NLL method and is shown in the first row (MAE of 0.693). We then study the effect of fixing one of the temperatures at non-zero value while setting the other temperature to 0. With $T_2 = 100, T_3 = 0$, we see slight improvement in regression performance (MAE of 0.614 vs. 0.693) and much poorer performance with respect to uncertainty calibration (UCE of 1.169 vs. 0.581), this is due to more weighting of fidelity term between the prediction and the ground-truth along with suppression of the default calibration effect of NLL. On the other hand, $T_2 = 0, T_3 = 100$ suppresses the default fidelity term for NLL, therefore the output is of significantly worse quality (poor regression scores, MAE of 1.395 vs 0.693) this further degrades the quality of the uncertainty estimates (UCE 3.733 vs 0.581). We notice that if the model does not perform good regression, the quality of uncertainty estimate is also adversely effected.

Methods	Metrics									
	MAE ↓	MSE ↓	PSNR ↑	SSIM ↑	C.Coeff. ↑	UCE ↓	R.UCE ↓	Log-likeli. ↑	ECE ↓	Sharp. ↓
$T_2 = 0, T_3 = 0$	0.693	0.414	37.15	0.955	0.189	0.581	0.512	-0.36	1.45	2.73
$T_2 = 100, T_3 = 0$	0.614	0.384	37.72	0.961	0.062	1.169	0.833	-0.41	1.77	2.82
$T_2 = 0, T_3 = 100$	1.395	7.274	20.19	0.793	0.219	3.733	2.442	-0.44	2.12	3.11
$T_2 = \downarrow, T_3 = 0$	0.612	0.344	37.76	0.961	0.077	0.983	0.797	-0.27	1.03	1.35
$T_2 = 0, T_3 = \downarrow$	0.632	0.388	37.71	0.960	0.442	0.152	0.116	-0.20	0.85	0.98
$T_2 = \downarrow, T_3 = \downarrow$	0.618	0.351	37.87	0.962	0.518	0.104	0.083	-0.16	0.74	0.83
$T_2 = \downarrow, T_3 = \downarrow$ with $P(\theta) = \mathcal{N}(\theta)$	0.625	0.358	36.98	0.952	0.488	0.168	0.133	-0.24	1.12	1.47
$T_2 = \downarrow, T_3 = \downarrow$ with $P(\theta) = \mathcal{E}(\theta)$	0.612	0.353	37.92	0.966	0.503	0.118	0.102	-0.15	0.83	1.01

Table 2: Ablation study of temperature hyperparameters of the temperature dependent posterior used in the proposed *posterior annealing* (POSTA) method on image super-resolution task.

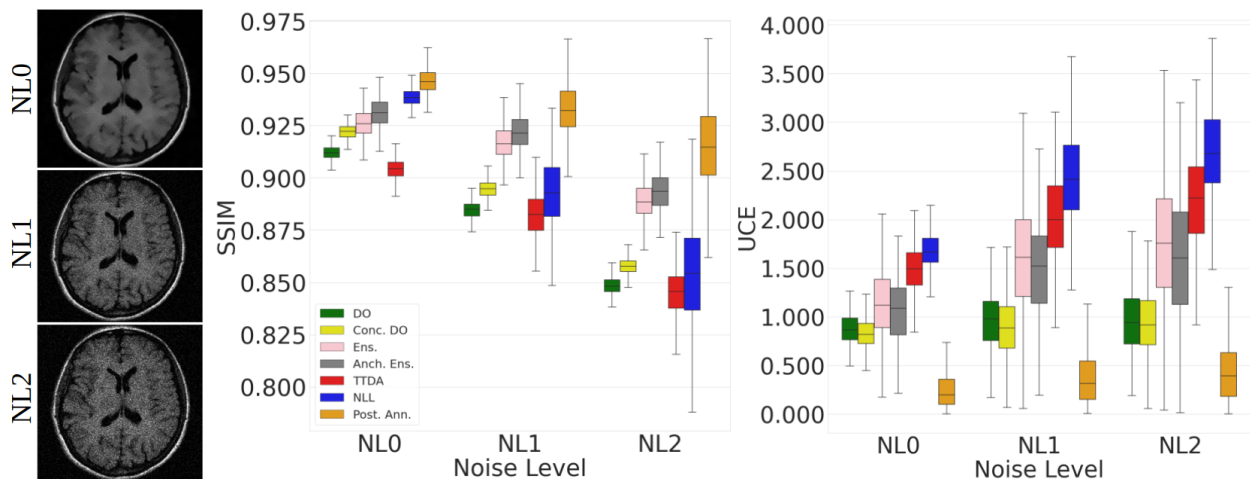


Figure 6: Evaluation of different methods using out-of-distribution input samples for MRI translation.

We then study the effects of decaying one of the temperatures while setting other to 0. With T_2 decaying (i.e., $T_2 = \downarrow, T_3 = 0$) we see slightly better performance than $T_2 = 100, T_3 = 0$ (MAE of 0.612 vs. 0.614 and UCE of 0.983 vs. 1.169), whereas with T_2 decaying (i.e., $T_2 = 0, T_3 = \downarrow$) we see good regression performance but also an improved calibration performance (UCE of 0.152 vs. 0.581). With both the parameters decaying (i.e., $T_2 = \downarrow, T_3 = \downarrow$) we achieve improved regression and calibration results concluding that annealing works the best. In addition to uniform prior setup (i.e., $P(\theta) = \mathcal{U}(\theta)$), we evaluate two other priors (i) Gaussian prior on the parameters of the network, i.e., $P(\theta) = \mathcal{N}(\theta)$ that is equivalent to ℓ_2 regularization of weights and (ii) Laplace prior, i.e., $P(\theta) = \mathcal{E}(\theta)$ that is equivalent to ℓ_1 regularization of weights. With Gaussian/Laplace prior we achieve MAE of 0.625/0.612 showing that carefully crafted priors may further boost the performance, designing such priors will be explored in future works.

4.4 Evaluation on Out-of-Distribution Data

Previous works have studied the performance of various uncertainty-aware methods in the presence of out-of-distribution (OOD) samples at the inference time (Ovadia et al., 2019; Hendrycks et al., 2019; Nandy et al., 2020; Mundt et al., 2019). To evaluate if better quality of uncertainty estimates lead to better OOD performance, we evaluate all the uncertainty trained model for MRI Translation on OOD samples. MRI image acquisition is a noisy process that leads to noisy/corrupted images (Macovski, 1996; Parrish et al., 2000; Wiest-Daesslé et al., 2008; Aja-Fernández & Vegas-Sánchez-Ferrero, 2016). Similar to (Upadhyay et al., 2021a;c; Sudarshan et al., 2021), we study the performance of various uncertainty-aware models in the presence of noisy input samples (corrupted with varying degrees of noise) at test time. Figure 6-(left) shows the example of in-distribution (noise-level 0, NL0) and out-of-distribution samples (NL1 and NL2).

The severity of corruption gradually increases from NL0 to NL2. From Figure 6-(middle and right), that shows the regression and quality of uncertainty estimates in the presence of OOD samples, we observe that the performance of various models degrades as severity of corruption increases from NL0 to NL2, however our POSTA method performs much better than the compared methods even at higher severity of corruption both in terms of regression and uncertainty calibration metric.

5 Conclusion

In this paper, we present a temperature dependent posterior to learn faster, better-calibrated uncertainty estimates for regression tasks. Our formulation speeds up model convergence and improves calibration of uncertainty without any post-hoc calibration phase. By annealing the temperature during training, we show that our method achieves 1.5 to 6 times faster convergence compared to other methods. Moreover, we demonstrate that our method achieves strong regression results while providing better calibrated uncertainty estimates compared to five uncertainty estimation methods on multiple regression datasets. Lastly, we present insights of our method with ablation study and show its potential to generalize well on out-of-distribution data, which further suggests its robustness.

References

- Santiago Aja-Fernández and Gonzalo Vegas-Sánchez-Ferrero. Statistical analysis of noise in mri. *Switzerland: Springer International Publishing*, 2016.
- Murat Seckin Ayhan and Philipp Berens. Test-time data augmentation for estimation of heteroscedastic aleatoric uncertainty in deep neural networks. 2018.
- David A Belsley, Edwin Kuh, and Roy E Welsch. *Regression diagnostics: Identifying influential data and sources of collinearity*, volume 571. John Wiley & Sons, 2005.
- Victor Besnier, Andrei Bursuc, David Picard, and Alexandre Briot. Triggering failures: Out-of-distribution detection by learning from local adversarial attacks in semantic segmentation. In *Proceedings of the IEEE/CVF International Conference on Computer Vision*, 2021.
- Charles Blundell, Julien Cornebise, Koray Kavukcuoglu, and Daan Wierstra. Weight uncertainty in neural network. In *International Conference on Machine Learning*, pp. 1613–1622. PMLR, 2015.
- Haoxian Chen, Ziyi Huang, Henry Lam, Huajie Qian, and Haofeng Zhang. Learning prediction intervals for regression: Generalization and calibration. In *International Conference on Artificial Intelligence and Statistics*. PMLR, 2021.
- Tianqi Chen, Emily Fox, and Carlos Guestrin. Stochastic gradient hamiltonian monte carlo. In *International conference on machine learning*, pp. 1683–1691. PMLR, 2014.
- Youngseog Chung, Willie Neiswanger, Ian Char, and Jeff Schneider. Beyond pinball loss: Quantile methods for calibrated uncertainty quantification. *Advances in Neural Information Processing Systems*, 2021.
- Peng Cui, Wenbo Hu, and Jun Zhu. Calibrated reliable regression using maximum mean discrepancy. *Advances in Neural Information Processing Systems*, 33, 2020.
- Erik Daxberger, Agustinus Kristiadi, Alexander Immer, Runa Eschenhagen, Matthias Bauer, and Philipp Hennig. Laplace redux-effortless bayesian deep learning. *Advances in Neural Information Processing Systems*, 34, 2021.
- Shai Feldman, Stephen Bates, and Yaniv Romano. Improving conditional coverage via orthogonal quantile regression. *Advances in Neural Information Processing Systems*, 2021.
- Gianni Franchi, Andrei Bursuc, Emanuel Aldea, Séverine Dubuisson, and Isabelle Bloch. Tradi: Tracking deep neural network weight distributions. In *European Computer Vision Conference*, 2020.

-
- Yarin Gal. Uncertainty in deep learning. 2016.
- Yarin Gal and Zoubin Ghahramani. Dropout as a bayesian approximation: Representing model uncertainty in deep learning. In *international conference on machine learning*, 2016.
- Yarin Gal, Jiri Hron, and Alex Kendall. Concrete dropout. In I. Guyon, U. Von Luxburg, S. Bengio, H. Wallach, R. Fergus, S. Vishwanathan, and R. Garnett (eds.), *Advances in Neural Information Processing Systems*, 2017.
- Victor Garcia Satorras, Zeynep Akata, and Max Welling. Combining generative and discriminative models for hybrid inference. In *33rd Conference on Neural Information Processing Systems*, pp. 1–11. Curran Associates, Inc., 2019.
- Jakob Gawlikowski, Cedric R. Njietcheu Tassi, Mohsin Ali, Jongseok Lee, Matthias Humt, Jianxiang Feng, Anna Kruspe, Rudolph Triebel, Peter Jung, Ribana Roscher, et al. A survey of uncertainty in deep neural networks. *arXiv preprint arXiv:2107.03342*, 2021.
- Christina Gillmann, Dorothee Saur, Thomas Wischgoll, and Gerik Scheuermann. Uncertainty-aware visualization in medical imaging—a survey. In *Computer Graphics Forum*. Wiley Online Library, 2021.
- Alex Graves. Practical variational inference for neural networks. *Advances in neural information processing systems*, 24, 2011.
- Chuan Guo, Geoff Pleiss, Yu Sun, and Kilian Q Weinberger. On calibration of modern neural networks. In *International Conference on Machine Learning*, pp. 1321–1330. PMLR, 2017.
- David Harrison Jr and Daniel L Rubinfeld. Hedonic housing prices and the demand for clean air. *Journal of environmental economics and management*, 5(1):81–102, 1978.
- Dan Hendrycks, Kimin Lee, and Mantas Mazeika. Using pre-training can improve model robustness and uncertainty. In *International Conference on Machine Learning*, 2019.
- Eyke Hüllermeier and Willem Waegeman. Aleatoric and epistemic uncertainty in machine learning: An introduction to concepts and methods. *Machine Learning*, 2021.
- Andrey Ignatov, Radu Timofte, et al. Pirm challenge on perceptual image enhancement on smartphones: report. In *European Conference on Computer Vision (ECCV) Workshops*, January 2019.
- Alex Kendall and Yarin Gal. What uncertainties do we need in bayesian deep learning for computer vision? *Advances in Neural Information Processing Systems*, 30:5574–5584, 2017.
- Diederik P Kingma and Jimmy Ba. Adam: A method for stochastic optimization. *arXiv preprint arXiv:1412.6980*, 2014.
- Michael Kläs and Anna Maria Vollmer. Uncertainty in machine learning applications: A practice-driven classification of uncertainty. In *International conference on computer safety, reliability, and security*, 2018.
- Volodymyr Kuleshov, Nathan Fenner, and Stefano Ermon. Accurate uncertainties for deep learning using calibrated regression. In *International Conference on Machine Learning*, pp. 2796–2804. PMLR, 2018.
- Balaji Lakshminarayanan, Alexander Pritzel, and Charles Blundell. Simple and scalable predictive uncertainty estimation using deep ensembles. *arXiv preprint arXiv:1612.01474*, 2016.
- Max-Heinrich Laves, Sontje Ihler, Jacob F Fast, Lüder A Kahrs, and Tobias Ortmaier. Well-calibrated regression uncertainty in medical imaging with deep learning. In *Medical Imaging with Deep Learning*, pp. 393–412. PMLR, 2020.
- Christian Leibig, Vaneeda Allken, Murat Seçkin Ayhan, Philipp Berens, and Siegfried Wahl. Leveraging uncertainty information from deep neural networks for disease detection. *Scientific reports*, 2017.

-
- Dan Levi, Liran Gispan, Niv Giladi, and Ethan Fetaya. Evaluating and calibrating uncertainty prediction in regression tasks. *arXiv preprint arXiv:1905.11659*, 2019.
- Zhen Lin, Shubhendu Trivedi, and Jimeng Sun. Locally valid and discriminative prediction intervals for deep learning models. *Advances in Neural Information Processing Systems*, 2021.
- Albert Macovski. Noise in mri. *Magnetic resonance in medicine*, 1996.
- Wesley J Maddox, Pavel Izmailov, Timur Garipov, Dmitry P Vetrov, and Andrew Gordon Wilson. A simple baseline for bayesian uncertainty in deep learning. *Advances in Neural Information Processing Systems*, 2019.
- Alireza Mehrtash, Purang Abolmaesumi, Polina Golland, Tina Kapur, Demian Wassermann, and William M Wells III. Pep: Parameter ensembling by perturbation. *Advances in Neural Information Processing Systems*, 2020.
- Martin Mundt, Iuliia Pliushch, Sagnik Majumder, and Visvanathan Ramesh. Open set recognition through deep neural network uncertainty: Does out-of-distribution detection require generative classifiers? In *Proceedings of the IEEE/CVF International Conference on Computer Vision Workshops*, 2019.
- Jay Nandy, Wynne Hsu, and Mong Li Lee. Towards maximizing the representation gap between in-domain & out-of-distribution examples. *Advances in Neural Information Processing Systems*, 2020.
- Yaniv Ovadia, Emily Fertig, Jie Ren, Zachary Nado, David Sculley, Sebastian Nowozin, Joshua Dillon, Balaji Lakshminarayanan, and Jasper Snoek. Can you trust your model’s uncertainty? evaluating predictive uncertainty under dataset shift. *Advances in neural information processing systems*, 2019.
- Todd B Parrish, Darren R Gitelman, Kevin S LaBar, and M-Marsel Mesulam. Impact of signal-to-noise on functional mri. *Magnetic Resonance in Medicine*, 2000.
- Tim Pearce, Alexandra Brintrup, Mohamed Zaki, and Andy Neely. High-quality prediction intervals for deep learning: A distribution-free, ensembled approach. In *International Conference on Machine Learning*, pp. 4075–4084. PMLR, 2018.
- Tim Pearce, Felix Leibfried, and Alexandra Brintrup. Uncertainty in neural networks: Approximately bayesian ensembling. In *AISTATS*, 2020.
- Buu Phan, Rick Salay, Krzysztof Czarnecki, Vahdat Abdelzad, Taylor Denouden, and Sachin Vernekar. Calibrating uncertainties in object localization task. *arXiv preprint arXiv:1811.11210*, 2018.
- Emma C Robinson, Alexander Hammers, Anders Ericsson, A David Edwards, and Daniel Rueckert. Identifying population differences in whole-brain structural networks: a machine learning approach. *NeuroImage*, 50(3):910–919, 2010.
- Yaniv Romano, Evan Patterson, and Emmanuel Candes. Conformalized quantile regression. *Advances in neural information processing systems*, 2019.
- Olaf Ronneberger, Philipp Fischer, and Thomas Brox. U-net: Convolutional networks for biomedical image segmentation. In *International Conference on Medical image computing and computer-assisted intervention*, pp. 234–241. Springer, 2015.
- Sina Shafaei, Stefan Kugele, Mohd Hafeez Osman, and Alois Knoll. Uncertainty in machine learning: A safety perspective on autonomous driving. In *International Conference on Computer Safety, Reliability, and Security*, 2018.
- Hao Song, Tom Diethe, Meelis Kull, and Peter Flach. Distribution calibration for regression. In *International Conference on Machine Learning*, pp. 5897–5906. PMLR, 2019.
- Viswanath P Sudarshan, Uddeshya Upadhyay, Gary F Egan, Zhaolin Chen, and Suyash P Awate. Towards lower-dose pet using physics-based uncertainty-aware multimodal learning with robustness to out-of-distribution data. *Medical Image Analysis*, 73:102187, 2021.

-
- Natasa Tagasovska and David Lopez-Paz. Single-model uncertainties for deep learning. *Advances in Neural Information Processing Systems*, 32:6417–6428, 2019.
- Radu Timofte, Shuhang Gu, Jiqing Wu, Luc Van Gool, Lei Zhang, Ming-Hsuan Yang, Muhammad Haris, et al. Ntire 2018 challenge on single image super-resolution: Methods and results. In *The IEEE Conference on Computer Vision and Pattern Recognition (CVPR) Workshops*, June 2018.
- Raphael JL Townshend, Martin Vögele, Patricia Suriana, Alexander Derry, Alexander Powers, Yianni Laloudakis, Sidhika Balachandar, Bowen Jing, Brandon Anderson, Stephan Eismann, et al. Atom3d: Tasks on molecules in three dimensions. *arXiv preprint arXiv:2012.04035*, 2020.
- Uddeshya Upadhyay, Yanbei Chen, and Zeynep Akata. Robustness via uncertainty-aware cycle consistency. *Advances in Neural Information Processing Systems*, 2021a.
- Uddeshya Upadhyay, Yanbei Chen, Tobias Hepp, Sergios Gatidis, and Zeynep Akata. Uncertainty-guided progressive gans for medical image translation. In *International Conference on Medical Image Computing and Computer-Assisted Intervention*, 2021b.
- Uddeshya Upadhyay, Viswanath P Sudarshan, and Suyash P Awate. Uncertainty-aware gan with adaptive loss for robust mri image enhancement. In *Proceedings of the IEEE/CVF International Conference on Computer Vision*, pp. 3255–3264, 2021c.
- Uddeshya Upadhyay, Shyamgopal Karthik, Yanbei Chen, Massimiliano Mancini, and Zeynep Akata. Bayescap: Bayesian identity cap for calibrated uncertainty in frozen neural networks. In *Computer Vision—ECCV 2022: 17th European Conference, Tel Aviv, Israel, October 23–27, 2022, Proceedings, Part XII*, pp. 299–317. Springer, 2022.
- Kush R Varshney and Homa Alemzadeh. On the safety of machine learning: Cyber-physical systems, decision sciences, and data products. *Big data*, 2017.
- Guotai Wang, Wenqi Li, Michael Aertsen, Jan Deprest, Sébastien Ourselin, and Tom Vercauteren. Aleatoric uncertainty estimation with test-time augmentation for medical image segmentation with convolutional neural networks. *Neurocomputing*, 2019.
- Zhou Wang, Alan C Bovik, Hamid R Sheikh, and Eero P Simoncelli. Image quality assessment: from error visibility to structural similarity. *IEEE transactions on image processing*, 13(4):600–612, 2004.
- Max Welling and Yee W Teh. Bayesian learning via stochastic gradient langevin dynamics. In *Proceedings of the 28th international conference on machine learning (ICML-11)*, pp. 681–688. Citeseer, 2011.
- Nicolas Wiest-Daesslé, Sylvain Prima, Pierrick Coupé, Sean Patrick Morrissey, and Christian Barillot. Rician noise removal by non-local means filtering for low signal-to-noise ratio mri: applications to dt-mri. In *International Conference on Medical Image Computing and Computer-assisted Intervention*, 2008.
- Wenda Xu, Jia Pan, Junqing Wei, and John M Dolan. Motion planning under uncertainty for on-road autonomous driving. In *2014 IEEE International Conference on Robotics and Automation (ICRA)*, 2014.
- Xing Yan, Weizhong Zhang, Lin Ma, Wei Liu, and Qi Wu. Parsimonious quantile regression of financial asset tail dynamics via sequential learning. *Advances in neural information processing systems*, 2018.
- Tianhui Zhou, Yitong Li, Yuan Wu, and David Carlson. Estimating uncertainty intervals from collaborating networks. *Journal of Machine Learning Research*, 2021.